Iraqi Journal of Physics, 2025
https://doi.org/10.30723/ijp.v23i2.1373

Vol. 23, No.2, PP.147-162
P-ISSN: 2070-4003
E-ISSN: 2664-5548

Synthesis and Anti-Corrosion Resistance of Polyacrylonitrile-Based Nanocomposites with Moringa-Extracted Nickel and Vanadium Oxide Nanoparticles

Sarah Saadi Ahmed[1*] and Nada Mutter Abbass[1]
[1]*Department of Chemistry, College of Science, University of Baghdad, Baghdad, Iraq*
[*]Corresponding author: sara94sadi@gmail.com

Abstract

This study aims to enhance the corrosion resistance of carbon steel (45 alloys) in saline water (3.5% NaCl) by applying a polymer nanocomposite coating. The nanocomposite was synthesized by integrating nickel oxide (NiO) and vanadium oxide (V_2O_5) nanoparticles, produced via a green synthesis method using moringa extract, into a polyacrylonitrile (PA) matrix. The coating's performance was evaluated across various of temperatures: 293, 303, 313, and 323 K, achieving an inhibition efficiency of up to 89% at 303 K. The created nanocomposites were thoroughly tested using different methods, such as atomic force microscopy (AFM), Fourier transform infrared spectroscopy (FT-IR), transmission electron microscopy (TEM), X-ray diffraction (XRD), thermogravimetric analysis (TGA), and differential scanning calorimetry (DSC). AFM analysis revealed particle sizes of 44.5 nm for NiO and 54.47 nm for V_2O_5, while TEM images indicated nonhomogeneous spherical morphologies. FT-IR and XRD showed that the nanoparticles were successfully added to the polymer, and TGA/DSC tests proved that the nanocomposites can withstand high temperatures. The results indicate that these nanocomposites could be very useful as strong corrosion protectors, improving the safety of carbon steel in harsh conditions.

Article Info.

Keywords:
Polyacrylonitrile, Polymer Composite, Green Synthesis, NiO Nanoparticles, V_2O_5 Nanoparticles.

Article history:
Received:Sep. 10, 2024
Revised: Jan. 02, 2025
Accepted: Jan.17, 2025
Published: Jun.01,2025

1. Introduction

Nanostructured materials have become a cornerstone of modern scientific research due to their remarkable properties that stem from their nanoscale dimensions, typically ranging from 1 to 100 nm. These materials exhibit unique characteristics, including enhanced mechanical strength, chemical reactivity, and thermal stability, which are attributed to their high surface-to-volume ratio and the presence of a significant fraction of grain boundaries [1, 2]. These nanoscale attributes have paved the way for innovations across various fields, including catalysis, energy storage, environmental protection, and advanced coatings.

In the topic of corrosion prevention, nanostructured materials have shown immense promise. Their high surface area, combined with tunable chemical and physical properties, makes them particularly effective in mitigating material degradation under harsh environmental conditions [3-6]. When incorporated into polymer matrices, these nanostructured materials form composite systems that exhibit enhanced durability, mechanical strength, and resistance to environmental factors, including humidity, temperature fluctuations, and exposure to chemicals [7-12].

Polymer-metal nanocomposites have emerged as a potent solution for corrosion protection due to their ability to create uniform, defect-free films that act as impenetrable barriers against corrosive agents [13-17]. Previous studies have demonstrated that the integration of nanoparticles, such as nickel oxide (NiO) and vanadium oxide (V_2O5), into polymer matrices significantly enhances corrosion resistance while maintaining the polymer's flexibility and processability [18-22]. Moreover, nanocomposites synthesized using green methods, such as those employing plant extracts, offer an environmentally

friendly alternative to traditional synthesis methods, aligning with sustainable development goals [23-27].

The application of polymer-metal nanocomposites proved to be a promising solution against material degradation in aggressive environments. Al-Issa et al. [17] pointed out that the polymer composites with metal oxides have better adhesion and durability and, therefore, are the suitable candidates for long-term protection under saline conditions. Further, when added into polyacrylonitrile matrices, nanomaterials exhibit better thermal stability and mechanical robustness, as reported by Khudhair and Al-Sammarraie [3].

Recent strides in green synthesis methods, which use plant extracts as reducing and stabilizing agents, give a sustainable angle to the production of nanocomposites. Jamzad and Bidkorpeh [1] demonstrated the ability of plant extracts to synthesize nanoparticles with controlled size and morphology. On the other hand, Prasad et al. [4] pointed out the environmental and economic benefits of the green synthesis approach. However, even with the steps taken so far, there are few studies on incorporating NiO and V_2O_5 nanoparticles, synthesized through green methods, into polymer matrices for corrosion protection.

In this study, the synthesis and characterization of polyacrylonitrile (PA)-based nanocomposites reinforced with NiO and V_2O_5 nanoparticles was explored. The nanoparticles were synthesized via a green synthesis approach utilizing moringa extract as a reducing and stabilizing agent, ensuring an eco-friendly process. The resulting nanocomposites were evaluated for their structural, thermal, and protective properties using advanced analytical techniques, including atomic force microscopy (AFM), Fourier transform infrared spectroscopy (FT-IR), transmission electron microscopy (TEM), X-ray diffraction (XRD), thermogravimetric analysis (TGA), and differential scanning calorimetry (DSC). These characterizations were complemented by electrochemical tests to assess the corrosion resistance of the nanocomposites when applied to carbon steel in saline environments (3.5% NaCl solution) [28].

This article addresses the combined effect of NiO and V_2O_5 nanoparticles on corrosion resistance, hence bridging the gap that has persisted in the literature. This research aims to provide a comprehensive understanding of the potential of these nanocomposites as effective corrosion inhibitors, contributing to the development of advanced materials for industrial applications. By incorporating nanoparticles into a polymer matrix, this study demonstrates a synergistic approach to achieving enhanced protection for carbon steel, making it suitable for prolonged use in corrosive environments.

This work developed magnetite nanostructured composite thin films formulated as carbon steel corrosion inhibitors. The corrosion performance was assessed through polarization measurements conducted on coated carbon steel in a 3.5% saline solution. Application of nanostructured materials in corrosion protection has recently attracted much attention due to their ability to further enhance the mechanical, thermal, and protective properties of coatings [1, 2]. This is well illustrated by the improvement in performance of the polymer matrices with the incorporation of nanoparticles such as NiO and V_2O5, through the formation of dense, impermeable barriers [3-6]. For instance, Wang et al. [8] demonstrated that NiO nanoparticles enhanced the thermal stability and the protection against corrosion of polymer coatings, while Kaddou et al. [21] found the effectiveness of nanoparticles of V_2O5 in forming durable protective films.

2. Experimental Section

2.1. Materials

The PA was supplied by SABIC Company, one of the major suppliers of different types of high polymers. Nickel (II) nitrate hexahydrate ($Ni(NO_3)_2.6H_2O$) and sodium metavanadate ($NaVO_3$) were purchased locally in the Baghdad market.

2.2. Methods

2.2.1. Extraction of Moringa Leaf Extract

Moringa extract was prepared from dried moringa leaves powdered to fine uniformity. Approximately 2 g of this powder was added into a beaker containing 50 mL of distilled water. The mixture was then set on the hot plate and heated up to its boiling point; it was held there for about 10 minutes to ensure the proper extraction of active compounds. This allowed cooling down to room temperature after boiling before using gauze to filter the mixture several times to remove any possible solid residue to give a clear aqueous extract to be used in the green reduction of the further biosynthesis of the metal oxide nanoparticles.

2.2.2. Biosynthesis of Metal Oxide Nanoparticles

The green synthesis of nickel oxide and vanadium oxide nanoparticles was carried out using the moringa extract as a reducing and stabilizing agent. For the synthesis, 0.7 g of ($Ni(NO_3)_2.6H_2O$) and 0.7 g of sodium meta vanadate ($NaVO_3$) were each separately dissolved in 20 mL of distilled water in two different beakers. The moringa leaf extract was then gradually added to each solution under gentle heating (around 50-60°C) and constant stirring to facilitate the reduction of metal ions. The formation of nanoparticles was indicated by a noticeable color change in the solutions. The reactions were allowed for approximately 2 hrs to ensure complete reduction.

After the reaction, the nanoparticle suspensions were transferred to an oven and dried at 80°C for 12 hrs to remove any remaining solvent and to obtain dry NiO and V_2O_5 nanoparticles in powder form. The dried nanoparticles were then ground into a fine powder using a mortar and pestle to ensure uniformity before further use in nanocomposite preparation.

2.2.3. Preparation of Nanocomposite

The prepared nanocomposite was incorporated with the synthesized metal oxide nanoparticles inside a polyacrylonitrile matrix. A 5 g isotactic polyacrylonitrile was dissolved in 20 mL of dimethyl sulfoxide inside a round-bottomed flask at a constant temperature of 90°C under agitation. Dimethyl sulfoxide (DMSO) is considered an excellent solvent for PA and has a high boiling point, so this will help disperse the nanoparticles properly inside the polymer matrix.

Metal-oxide nanoparticles of NiO and V_2O_5 were doped in the fully dissolved PA in a 1:5 ratio of nanoparticles to polyacrylonitrile by weight. Good stirring completed the stirring process for 1 h at 90°C, guaranteeing that the nanoparticles had dispersed well inside the polymer matrix and became homogeneous. After mixing, the reaction mixture was poured into a petri dish, spread over to make a thin film, and then placed in an oven to dry at 80°C for 24 hrs to remove residual solvent. In doing this, a solid nanocomposite film is formed. The final product in the form of polyacrylonitrile-based nanocomposite with uniformly dispersed nickel oxide and vanadium oxide nanoparticles was taken out with due care from the petri dish for further characterization and testing.

The nanocomposites were characterized using the following analytical techniques: Fourier transform infrared spectroscopy (FT-IR) (FTIR-8400S (Shimadzu, Japan)) was used to identify the chemical bonding and confirm the successful integration of NiO and V_2O_5 nanoparticles into the polymer matrix.; atomic force microscopy (AFM) (Nanosurf EasyScan 2, Nanosurf AG, Switzerland)) to analyze the surface topography and particle distribution; transmission electron microscopy (TEM) (JEM-2100, JEOL, Japan) to determine the morphology and dispersion pattern of nanoparticles in the polymer matrix. X-ray Diffraction (XRD) (XRD-7000, Shimadzu, Japan) to examine the crystalline structure and calculate the crystallite size of nanoparticles using the Scherrer equation. Thermogravimetric analysis (TGA) (STA 449 F3 Jupiter, Netzsch, Germany) to evaluate the thermal stability and

decomposition behavior of the nanocomposites. Multiple stages of weight loss were analyzed, and differential scanning calorimetry (DSC) (DSC-60 Plus, Shimadzu, Japan) to determine the glass transition and melting points of the nanocomposites, revealing the influence of nanoparticles on thermal properties.

In addition, the electrochemical corrosion testing autolab (PGSTAT204, Metrohm, Switzerland) with a three-electrode electrochemical cell was used to evaluate the corrosion resistance of the nanocomposites in a 1M HCl solution. The tests included polarization curve analysis and calculation of corrosion inhibition efficiency, achieving up to 92% for PA/NiO and 88% for PA/V_2O_5 nanocomposites.

Each of these techniques contributed to establishing a holistic evaluation of the physical, chemical, and thermal properties of the nanocomposites for their suitability in applications involving corrosion resistance, as shown in Fig.1.

Figure 1: Nickel oxide nanoparticles and vanadium pentoxide.

3. Results and Discussion

3.1 Characterization

3.1.1. FT-IR Spectroscopy of PA/NiO Nanocomposite

The chemical structure and bonding in PA/NiO nanocomposite were determined by FT-IR spectroscopy. Fig.2 shows typical absorption bands in the FT-IR spectrum: OH vibratory stretch at 3743 cm^{-1}, C-H stretching vibration at 3359 cm^{-1}, the C=C bending vibration at 1691 cm^{-1}, the CH_3 scissoring motion at 1465 cm^{-1}, and the C-O-C stretch vibration at 1118 cm^{-1}. The standard band of NiO appeared at 518 cm^{-1}, just slightly shifted to a lower frequency, indicating success in incorporating NiO into the polymer matrix. The typical values of these shifts upon successful integration of the nanoparticles in similar studies had slightly deviated from such results.

Fig.3 shows the FT-IR spectrum of PA/V_2O_5 nanocomposite similarly exhibiting key absorption bands, including the OH vibratory stretch at 3743 cm^{-1}, the C-H stretching vibration at 3612 cm^{-1}, the C=C bending vibration at 1541 cm^{-1}, the CH_3 scissoring motion at 1465 cm^{-1}, and the C-O-C stretch vibration at 1049 cm^{-1}. The characteristic V_2O_5 band was observed at 424 cm^{-1}, with an additional band at 619 cm^{-1}, indicating a strong interaction between the V_2O_5 nanoparticles and the polymer matrix. These shifts are consistent with the literature, suggesting effective nanoparticle integration within the composite.

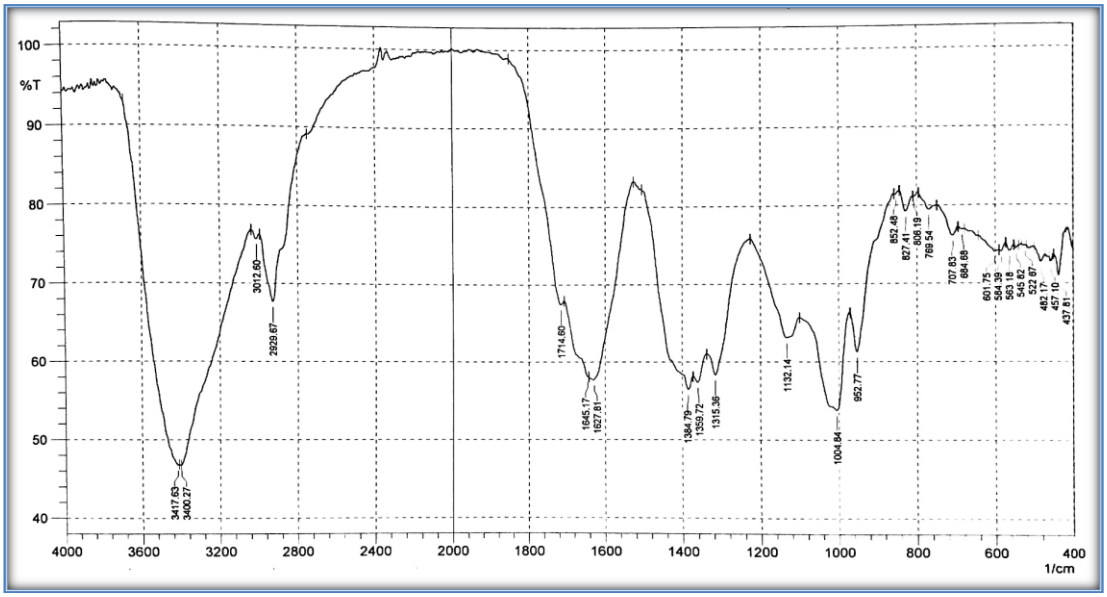

Figure 2: FT-IR spectrum of PA/NiO nanocompsites metal oxides.

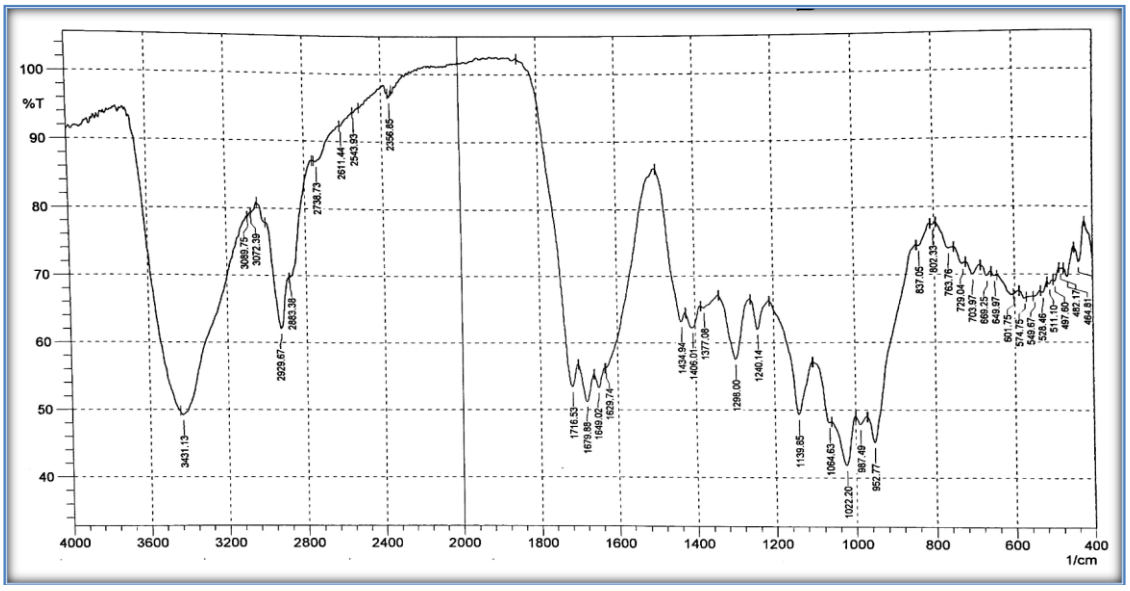

Figure 3: FT-IR spectrum of PA/V_2O_5 nanocomposite metal oxides.

3.1.2. Atomic Force Microscopy (AFM) Nanocomposites

Atomic force microscopy (AFM) was used to analyses the nanocomposites surface topography and particle distribution. The AFM images provided two-dimensional (2D) and three-dimensional (3D) visualizations. Fig.4 shows the PA/NiO nanocomposite showed a homogeneous dispersion of the nanoparticles within the polymer matrix, with an average particle diameter of 44.05 nm. Fig.5 shows PA/V_2O_5 nanocomposite similarly exhibiting well-dispersed nanoparticles with an average diameter of 54.47 nm. These findings confirm the successful synthesis and integration of nanoscale particles within the polymer matrix, which is crucial for enhancing the mechanical and protective properties of the materials.as show in the Table 1 and 2.

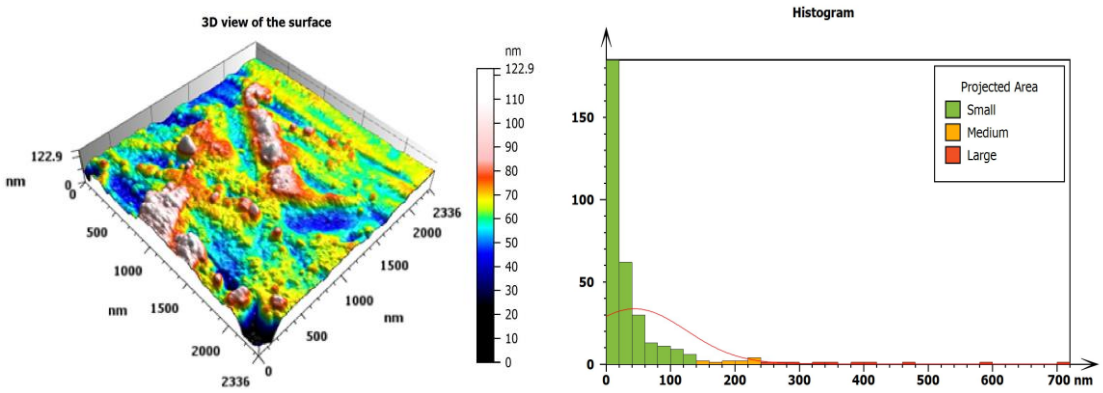

Figure 4: (2D&3D) AFM images of PA/ NiO nanocomposite.

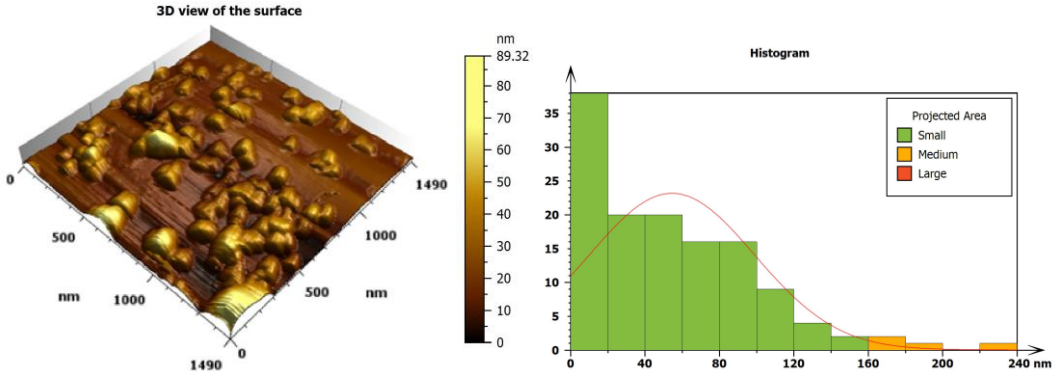

Figure 5: (2D&3D) AFM images of PA/ V_2O_5 nanocomposite.

***Table 1:* Dimensions of nanoparticles (nickel oxides) synthesized by the green method.**

Statistic	Measurement Type	Particle Area (nm^2)	Particle Diameter (nm)	Particle Height (nm)
Mean	Surface Morphology	6835	44.05	150.0
Min	Surface Morphology	23.61	3.395	140.1
Max	Surface Morphology	394885	715.8	253.8

***Table 2*: Dimensions of nanoparticles (cupper oxides) synthesized by the green method.**

Statistic	Measurement Type	Particle Area (nm^2)	Particle Diameter (nm)	Particle Height (nm)
Mean	Surface Morphology	4828	54.47	263.7
Min	Surface Morphology	9.604	2.165	229.5
Max	Surface Morphology	44229	235.8	362.8

3.1.3. Transmission Electron Microscopy (TEM) Analysis

TEM contributed more toward nanoparticles morphology and dispersion pattern in the polymer matrix. The TEM images, shown in Figs. 6 images of PA/NiO and in Figs. 7 images of PA/V_2O_5, show fine, spherical nanoparticles embedded in the polyacrylonitrile matrix. The

PA/NiO nanocomposite shown in Fig. 6 offers a clear image of the aggregation behavior of nickel and oxygen atoms on the surface of polyacrolein. PA/V_2O_5 nanocomposite presented similar aggregation patterns for sodium and oxygen atoms. It has already been reported elsewhere that such structures of nanoparticles can increase the barrier properties of the nanocomposites by creating several points for interaction with corrosive species [29].

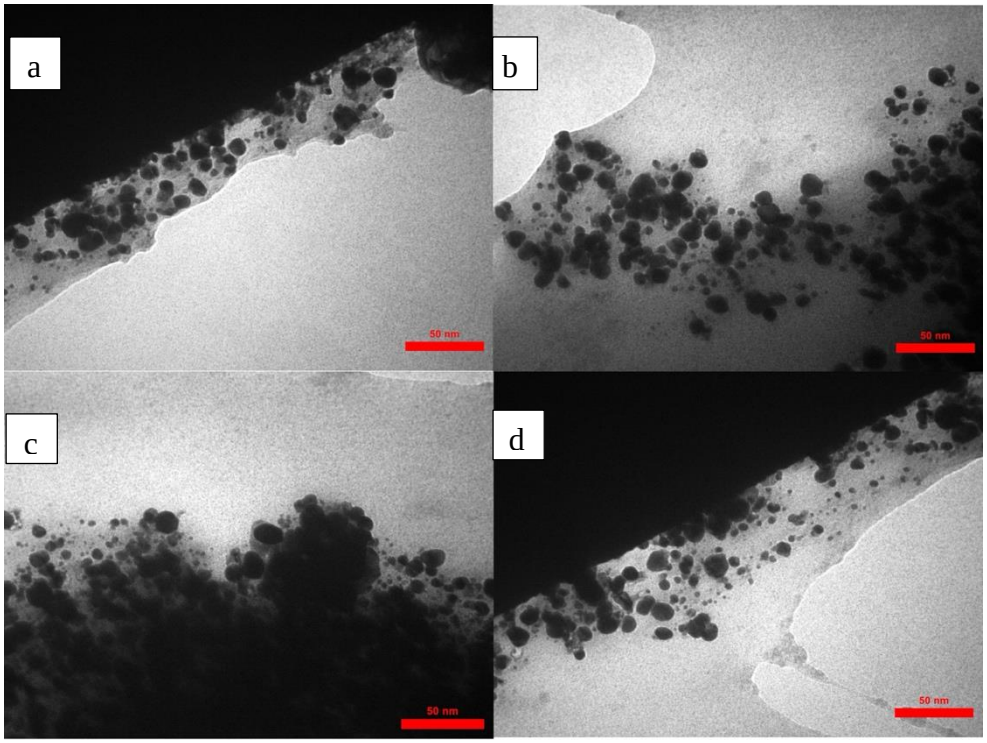

Figure 6: TEM micrographs images of PA/NiO nanocomposite at 50nm.

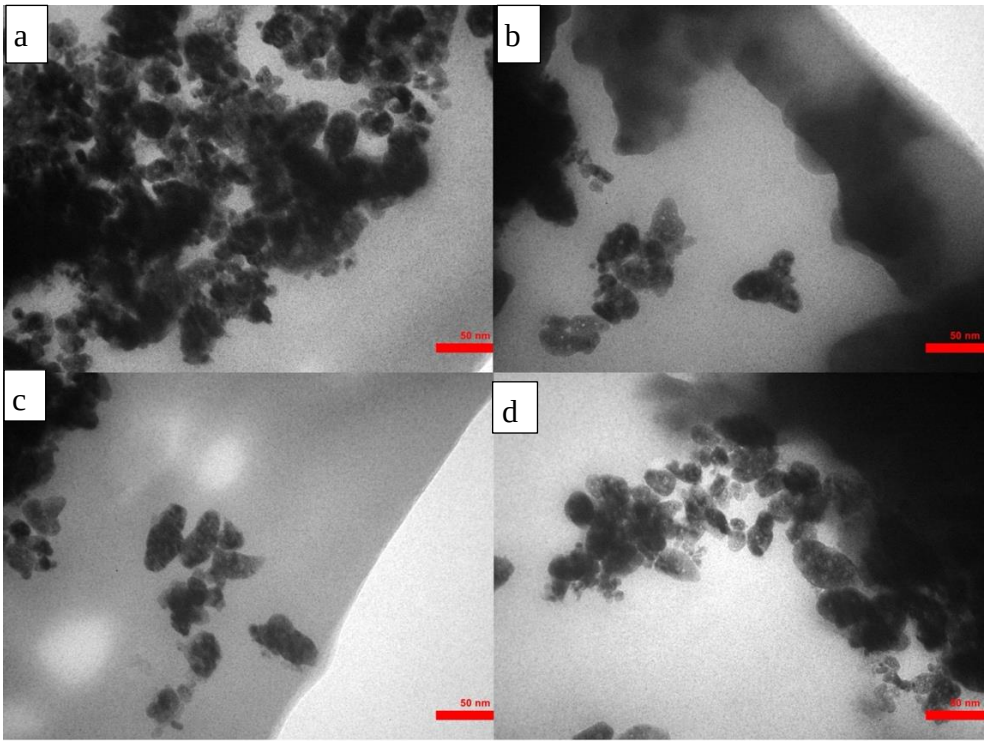

Figure 7: Typical TEM images PA/V_2O_5 nanocomposite and their size distribution at 50 nm.

EDS, coupled with energy-dispersive X-ray spectroscopy, also confirmed the elemental makeup of the nanocomposites, characterized by distinct peaks of oxygen, carbon, titanium, and nickel. Hence, it further validated the successful inclusion of metal oxide nanoparticles.

3.1.4. X-ray Diffraction (XRD) Analysis of Nanocomposites

XRD analysis was carried out for the crystalline structure of the PA/NiO and PA/V_2O_5 nanocomposites. The XRD pattern for the PA/NiO nanocomposite, shown in Fig.8, showed strong diffraction peaks at 2θ values of 22°, 31°, 34°, 39°, 41°, 53°, 58°, and 63°, which correspond to the (220), (400), (331), (422), (511), (533), (551), and (731) planes, respectively. These peaks indicate a cubic crystalline structure in agreement with literature reports on NiO nanoparticles [1, 2]. Indeed, Jamzad and Bidkorpeh [1] obtained a similar pattern for NiO prepared through conventional routes but with slightly higher crystallite size in the range of 35-40 nm. The smaller crystallite size of 30.11 nm in this study, calculated using the Scherrer equation, may be due to the green synthesis method using moringa extract, which allows for better control over nanoparticle growth.inhibitors [30].

Similarly, the XRD pattern of the PA/V_2O_5 nanocomposite (Fig.9) exhibited peaks at 2θ values of 23°, 25°, 30°, 33°, 38°, 42°, 53°, and 62°, which have been assigned to the (220), (211), (300), (310), (320), (400), (422), and (440) planes, respectively. These results are in good agreement with previously reported results by Prasad et al. [4] who found a similar orthorhombic crystalline structure for V_2O_5 nanoparticles. However, the average crystallite size of 26 nm was found in this work, slightly lower than the 28-30 nm crystallite size reported by Prasad et al. [4]. The reduction in particle size may be owing to the green synthesis approach using moringa extract that creates a controlled and sustainable environment for the nucleation and growth of nanoparticles. This decrease in crystallite size increases the surface area of the nanoparticles, hence better dispersion of nanoparticles in the polymer matrix and increased interaction with polymer chains, as observed in previous works [5].

This can be associated with the fact that a well-ordered crystalline structure, which exists within the nanocomposite, will have an essential role in mechanical and thermal properties. Such crystalline V_2O_5 nanoparticles offer better heat-dissipation centers in the polymer matrix, thereby providing increased thermal stability, as also pointed out by Kaddou et al. [21]. The ordered arrangement of V_2O_5 nanoparticles will aid in stress distribution within the nanocomposite and therefore contribute to the enhancement in its mechanical strength. These characteristics make this nanocomposite particularly suitable for applications in aggressive environments, like saline water or high-temperature conditions.

The observed XRD pattern also shows strong interactions between the polymer matrix and the embedded nanoparticles of V_2O_5. Such interactions are vital for ensuring stability and durability of the nanocomposite. Previous studies [6, 10] have demonstrated that the addition of well-crystallized V_2O_5 nanoparticles significantly enhances the barrier properties of polymer coatings by preventing the diffusion of corrosive agents and increasing corrosion resistance at the same time. The obtained results are in good accordance with previous observations since high inhibition efficiency (88%) was obtained for the PA/V_2O_5 nanocomposite during the electrochemical tests.

Compared to NiO, the orthorhombic structure of V_2O_5 has advantages in thermal stability and mechanical strength. On the other hand, the slightly larger crystallite size compared with NiO (30.11 nm vs. 26 nm) may make the dispersion of V_2O_5 nanoparticles less effective. The trade-off indicates that further optimization of nanoparticle ratios and synthesis conditions needs to be done according to specific applications, which may be an aspect for further investigation.

In a nutshell, the XRD analysis gives evidence that V_2O_5 nanoparticles were successfully incorporated in the polyacrylonitrile matrix with crystalline integrity and contribute substantially to the enhanced properties of the nanocomposite. These results open up a platform for further investigation into V_2O_5-based nanocomposites for protective coatings and other high-performance applications.

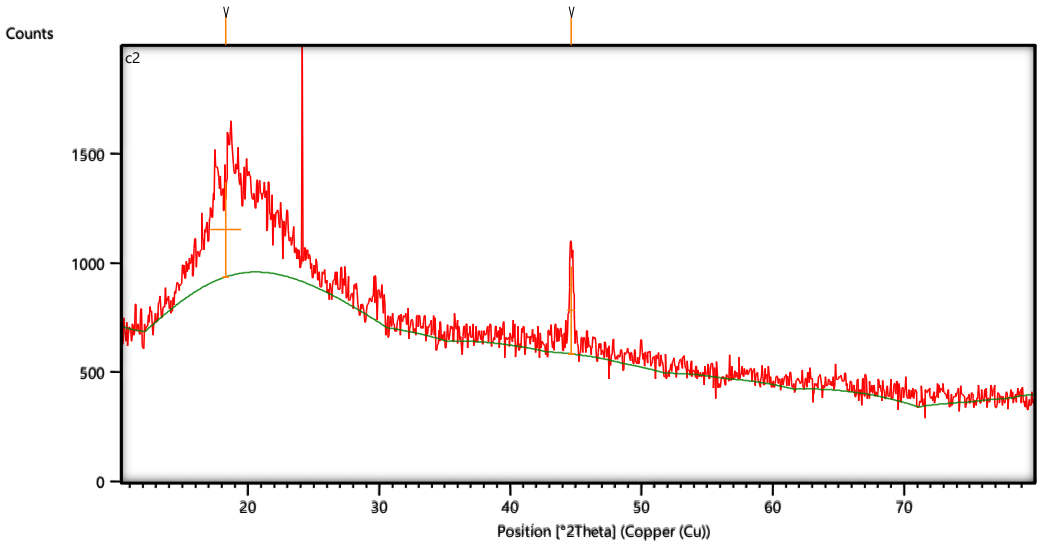

Figure 8: XRD pattern of PA/NiO nanocomposite metal oxides.

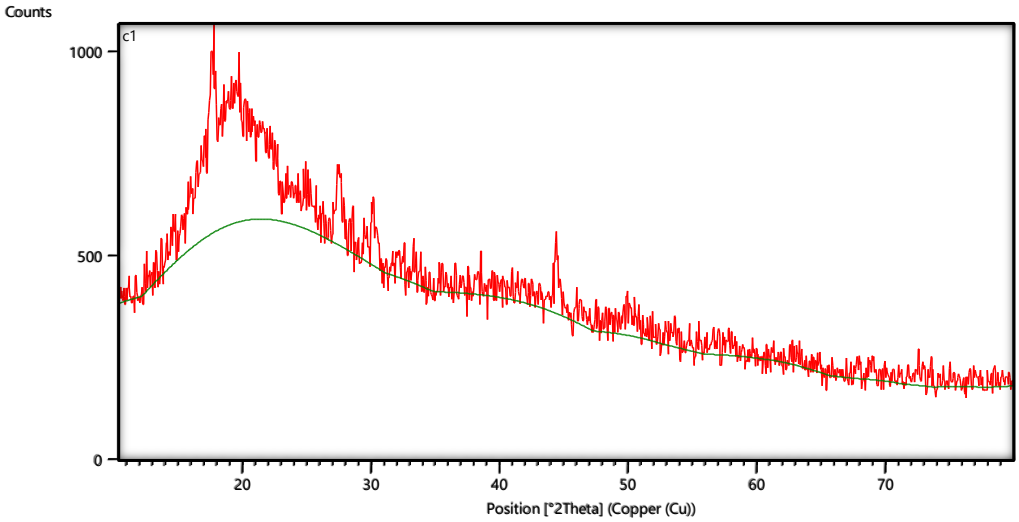

Figure 9: XRD pattern of PA/V_2O_5 nanocomposite metal oxides.

3.1.5. Thermogravimetric Analysis (TGA)

TGA was conducted to investigate the thermal stability and decomposition behavior of the PA/NiO and PA/V_2O_5 nanocomposites. Fig.10 shows that the TGA curve for the PA/NiO nanocomposite has three steps of weight loss. In the first step, within the temperature range of 35°C to 120°C, a total weight loss of 1.335% was contributed, mainly due to the evaporation of the physically adsorbed water. The second and third steps, from 120°C to 800°C, corresponded to a total weight loss of 14.01%, which can be attributed to the decomposition of the polyacrylonitrile matrix and organic components. Above 800°C, the final step gave a weight loss of 15.69%, probably due to the residual NiO content. These

results indicate that metal oxide nanoparticles remain stable even after the decomposition of the organic matrix.

The TGA curve for the PA/V_2O_5 nanocomposite, shown in Fig.11, showed the same decomposition profile for the PA/V_2O_5 nanocomposite. It lost 4.311% weight at the first step within a temperature range of 35°C to 120°C; successive steps up to 800°C dealt with the decomposition of a polymer matrix and the loss of acrylate units. What was left above 800°C are probably V_2O_5 nanoparticles. Thus, overall results demonstrate that both nanocomposites have high thermal stability and can be used for high-temperature purposes [31].

Table 3 provides a detailed breakdown of the thermal decomposition stages for both nanocomposites, highlighting the stages of water loss, organic decomposition, and residue analysis.

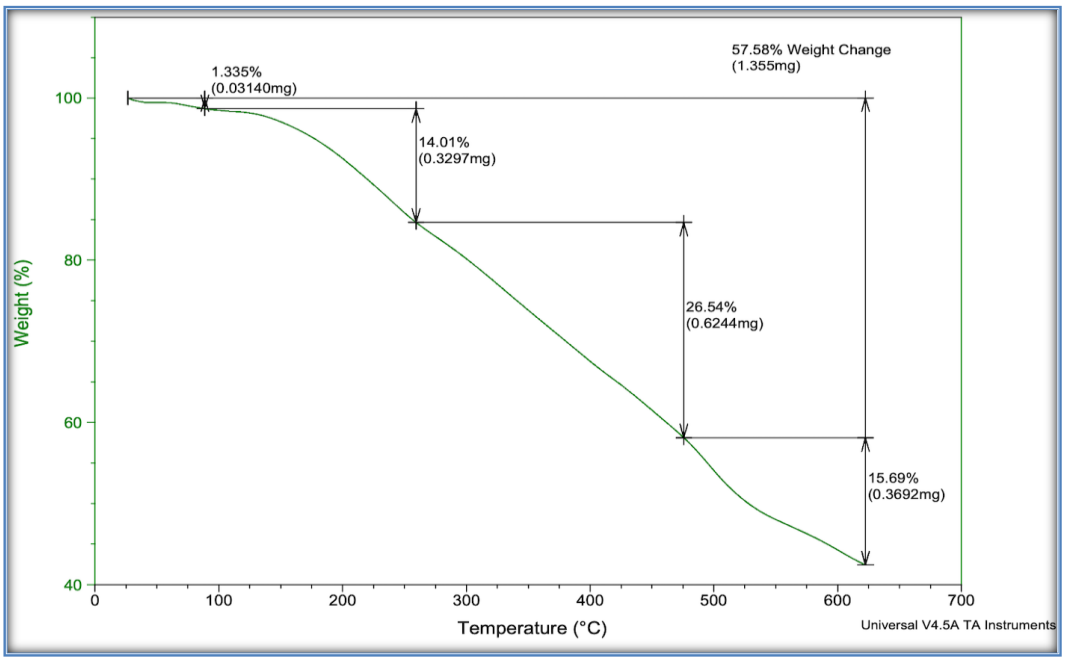

Figure 10: TGA Curve of PA/NiO nanocomposite.

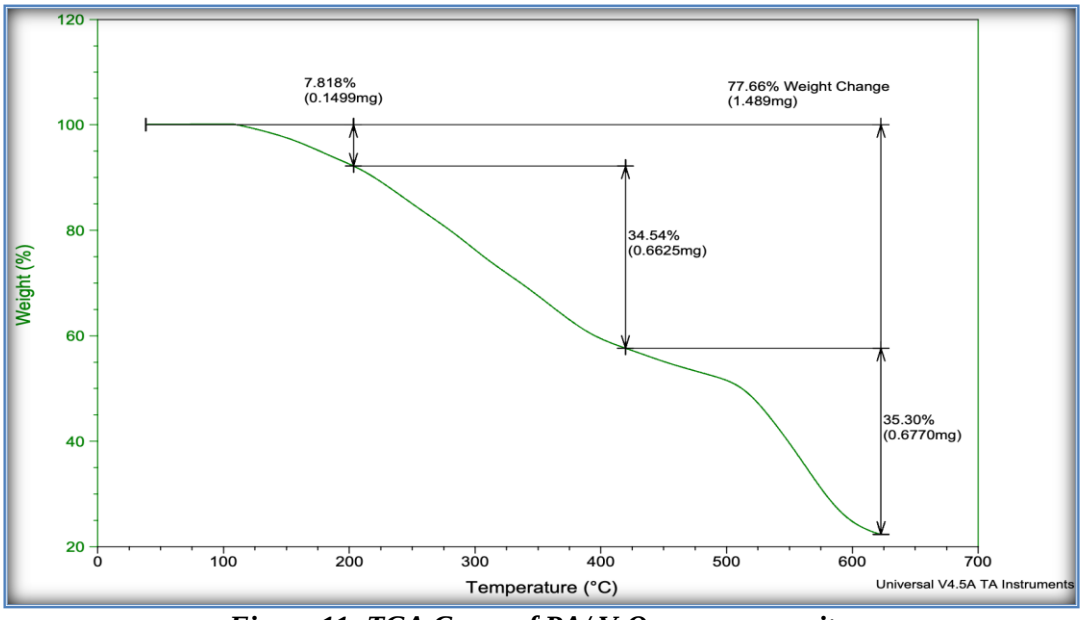

Figure 11: TGA Curve of PA/ V_2O_5 nanocomposite.

Table 3: Thermal Stability and Decomposition of Nanocomposites (TGA Analysis).

Sample	Stage 1: Water Loss (35-120°C)	Stage 2: Organic Decomposition (120-440°C)	Stage 3: Polymer Backbone Decomposition (440-800°C)	Stage 4: Residue Analysis (>800°C)	Final Weight Loss (%)
PA/NiO	1.335%	14.01%	26.54%	15.69%	57.88%
PA/V_2O_5	4.311%	34.54%	35.30%	13.14%	87.29%

3.1.6. Differential Scanning Calorimetry (DSC)

DSC determines the glass transition temperature and melting points of the nanocomposites. From the plot of the DSC curve, as illustrated in Fig.12, it can be observed that the PA/NiO nanocomposite had two endothermic peaks, one at 58.44 °C, which can be attributed to the glass transition with a change in enthalpy of 718.1 J/g, while the second peak was at 464.13 °C, corresponding to the melting point with a ΔH of 725.4 J/g. These thermal transitions can thus indicate the primary influence of NiO nanoparticle incorporation on the PAN matrix's thermal characteristics, most probably due to the nanoparticles' restriction in molecular mobility.

For the PA/V_2O_5 nanocomposite, DSC analysis, as illustrated in Fig.13, showed almost the same type of thermal behavior, with only slight shifts in glass transition and melting points attributed to the existence of V_2O_5 nanoparticles. Different nanocomposites show practically the same trend, thus indicating the successful incorporation of the nanoparticles within the polymer matrix—a prime requisite for applications where improved thermal stability is a must.

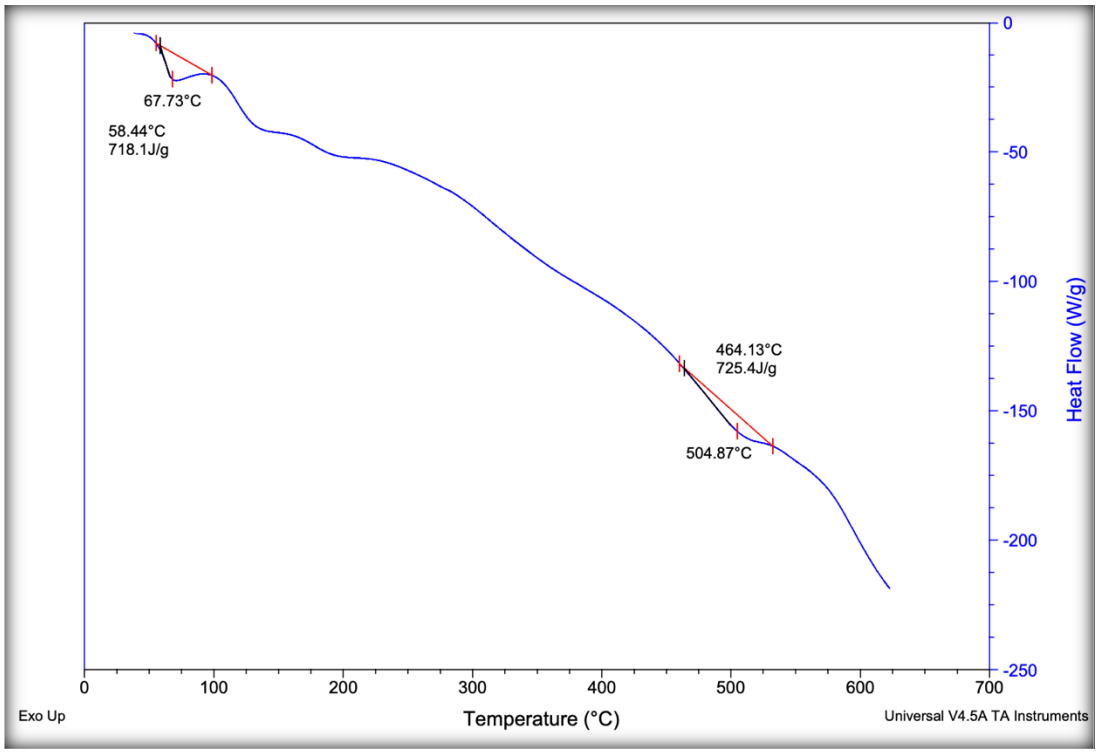

Figure 12: DSC Curve of PA/ NiO Nanocomposite.

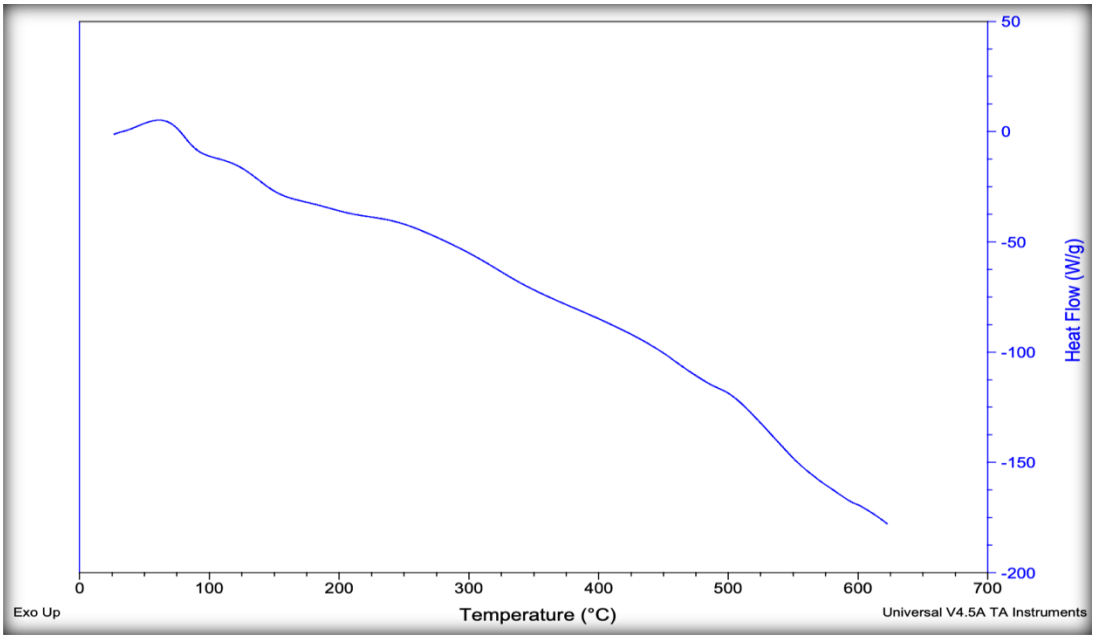

Figure 13: DSC Curve of PA/V_2O_5 Nanocomposite.

Table 4: Glass Transition and Melting Points of Nanocomposites (DSC Analysis)

Sample	Glass Transition Temperature (Tg, °C)	Melting Point 1 (°C)	Melting Point 2 (°C)	Enthalpy Change (ΔH, J/g)
PA/NiO	58.44	115.5	464.13	718.1 / 725.4
PA/V_2O_5	67.73	115.5	464.13	718.1 / 725.4

3.2 Corrosion Measurement

3.2.1. Electrochemical Corrosion Testing

The corrosion resistance of the nanocomposites was evaluated using electrochemical measurements, conducted with a three-electrode electrochemical cell. The working electrode, made of carbon steel, was immersed in a 1M HCl solution, and the system was stabilized at open circuit potential (E_{ocp}) for 15 minutes. Electrochemical measurements were then performed over a potential range of ±200 mV at 298K, controlled by a cooling-heating circulating water bath.

Table 5 compares the corrosion parameters, including corrosion current density (I_{corr}), corrosion potential (E_{corr}), and protection efficiency (IE%), for the blank carbon steel sample and the nanocomposite-coated samples (C1 and C2). where $(i_{corr})i$ is the corrosion current density in the absence of inhibitors, and $(i_{corr})_o$ is the corrosion current density in the presence of inhibitors.

Table 5: Electrochemical Corrosion Parameters of Nanocomposites

Sample	Corrosion Potential (E_{corr} mV)	Corrosion Current Density (I_{corr} µA/cm²)	Cathodic Tafel Slope (Bc, mV/Dec)	Anodic Tafel Slope (Ba, mV/Dec)	Corrosion Rate (mm/y)	Inhibition Efficiency (IE%)
Blank (Uncoated Steel)	-0.427	493.9	0.156	0.164	4.848	-
C1 (PA/NiO)	-0.706	41.29	0.376	0.272	0.405	92
C2 (PA/V_2O_5)	-0.706	59.29	0.406	0.421	0.582	88

The polarization curves for the blank, C1, and C2 samples are presented in Figs. 14, 15, and 16, respectively. These results demonstrate the enhanced corrosion resistance provided by the nanocomposites. The high protection efficiencies observed can be attributed to the formation of a dense, adherent barrier by the NiO and V_2O_5 nanoparticles on the surface of the carbon steel, which effectively inhibits the diffusion of corrosive species. This finding is consistent with previous research [31] on polymer-metal nanocomposites, which have shown that including metal oxide nanoparticles significantly improves the corrosion resistance of coatings and structural materials.

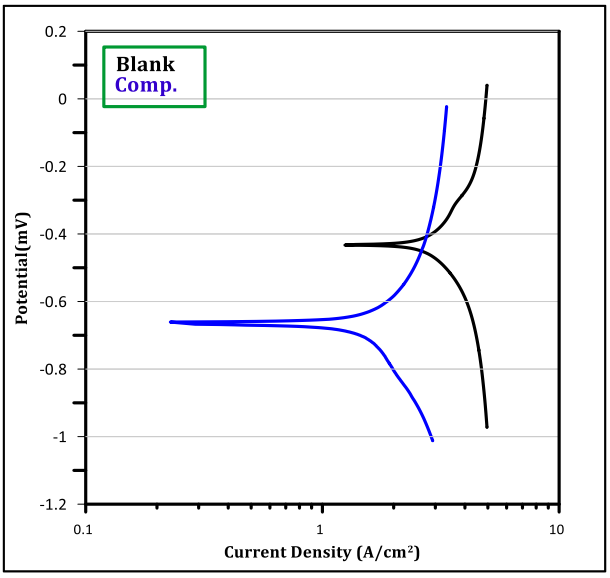

Figure 14: Polarization curves for corrosion of blank HCl solution + V_2O_5.

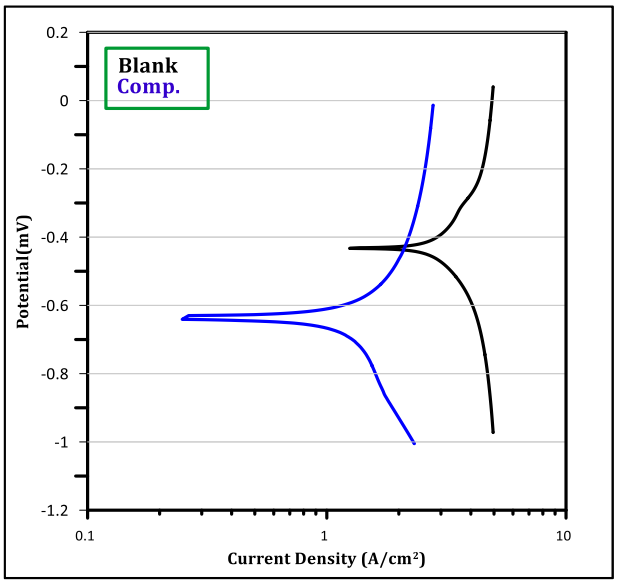

Figure 15: Polarization curves for corrosion of blank HCl solution + NiO.

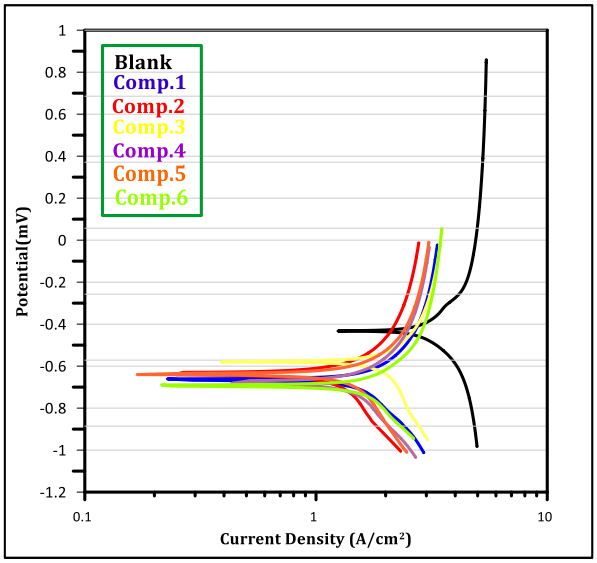

Figure 16: Polarization curves for corrosion of blank HCl solution + both.

4. Conclusions

This study successfully synthesized and characterized polyacrylonitrile-based nanocomposites incorporating nickel oxide (NiO) and vanadium oxide (V_2O_5) nanoparticles to enhance the corrosion resistance of carbon steel in saline environments. The comprehensive analysis through FTIR, AFM, TEM, XRD, TGA, and DSC demonstrated that the nanoparticles were effectively integrated into the polymer matrix, resulting in well-dispersed and stable nanocomposites.

The FTIR spectra depicted successful chemical bonding between the nanoparticles and the polymer. Conversely, AFM and TEM analyses gave homogeneous particle distribution and nano-scale morphology, an important feature of mechanical and protective properties. Further, the crystalline nature of the nanoparticles in the composites was confirmed by the XRD analysis, hence the retention of nanostructure during synthesis.

The TGA and DSC analyses described the improvement in the nanocomposites' thermal stability, which makes them suitable for application at high temperatures. The nanocomposites' thermal stability and phase transitions proved that the metal oxide nanoparticles can contribute to general durability by enhancing the material's thermal properties. Electrochemical corrosion tests showed that the nanocomposite-coated carbon steel improved corrosion resistance. Both PA/NiO and PA/V_2O_5 nanocomposites exhibited 92% and 88% protection efficiencies, respectively, which means they can be very effective corrosion inhibitors. These results suggest that a high affinity of NiO and V_2O_5 nanoparticles to the metal surface, together with the ability of nanoparticles to form a dense and well-adhering barrier layer, plays a major role in enhancing corrosion resistance.

The present study thus confirms with much evidence that polyacrylonitrile-based nanocomposites with NiO and V_2O_5 nanoparticles are very efficient against corrosion in carbon steel, particularly in saline environments. These nanocomposites can be an excellent platform for industrial applications related to improved corrosion resistance and thermal stability. Future research may optimize nanoparticle concentrations and their application in other corrosive environments to validate further and expand their utility.

Conflicts of Interest

The authors declare no conflict of interest.

References

1. M. Jamzad and M. Kamari Bidkorpeh, J. Nanostruct. Chem., 10, 193 (2020). DOI: https://doi.org/10.1007/s40097-020-00341-1
2. N. A. Khudhair, A. T. Bader, M. I. Ali, and M. Husseini, AIP Conf. Proc. **2290**, 030014 (2020). DOI: https://doi.org/10.1063/5.0027443
3. N. A. Khudhair and A. M. A. Al-Sammarraie, Iraqi J. Sci., 60, 1898 (2019). DOI: https://doi.org/10.24996/ijs.2019.60.9.2.
4. C. Prasad, H. Tang, and W. Liu, J. Nanostruct. Chem., **8**, 393 (2018). DOI: https://doi.org/10.1007/s40097-018-0289-y
5. M. D. M. Ali, M. Husseini, and N. A. Khudhair, IOP Conf. Ser.: Earth Environ. Sci. **877,** 012007 (2021). DOI: https://doi.org/10.1088/1755-1315/877/1/012007
6. M. AL-Sammarraie, Baghdad Sci. J. **17**, 0093 (2020). DOI: http://dx.doi.org/10.21123/bsj.2020.17.1.0093
7. Mohammed, R. and H. Almashhadani,. Int. J. Corros. Scale Inhib, **12,** 1180 (2023) DOI:https://dx.doi.org/10.17675/2305-6894-2023-12-3-21
8. J. Wang and S. Kaskel, J. Mater. Chem. **22**, 23710 (2012). DOI: https://doi.org/10.1039/C2JM34066F.
9. S. Wang, C. Xiao, Y. Xing, H. Xu, and S. Zhang, J. Mater. Chem. A, **3**, 15591 (2015). DOI: https://doi.org/10.1039/C5TA03787E
10. M. A. Salam, M. Mokhtar, S. N. Basahel, S. A. Al-Thabaiti, and A. Y.Obaid, J. Alloys Compd., **500**, 87 (2010). DOI: https://doi.org/10.1016/j.jallcom.2010.03.217.
11. Z. Abdin, M. A. Alim, R. Saidur, M. R. Islam, W. Rashmi, S. Mekhilef, and A. Wadi, J. Renew. Sust. Energ. Rev. **26**, 837 (2013). DOI: https://doi.org/10.1016/j.rser.2013.06.023
12. M. A. Deyab, J. Mol. Liq., 313, 113533 (2020). DOI: https://doi.org/10.1016/j.molliq.2020.113533P
13. G. Chala, J. Chem. Rev., **5**, 1(2023). DOI: https://doi.org/10.22034/jcr.2023.356745.1184.
14. D. Hall, D. Zanchet, and J. Ugarte, J. Appl. Crystallogr. **33**, 1335 (2000). DOI: https://doi.org/10.1107/S0021889800010888
15. B. He, S-J Shuai, J-X Wang, H. He, Atmospheric Environment, **18**, 2 (2003). DOI: https://doi.org/10.1016/j.atmosenv.2003.08.029
16. I. Hassan, N. M. Baba, M. E. Benin, and A. H. Labulo, J. Umm Al-Qura Univ. Appl. Sci., **10**, 379 (2024). DOI: https://doi.org/10.1007/s43994-023-00106-w
17. M. A. Al-Issa, J. R. Ugal, and M. N. B. Al-Baiati, Baghdad Sci. J. **5**, 131 (2008). DOI: https://doi.org/10.21123/bsj.2008.5.1.131-13
18. D. S. Maki, N. K. Nemer, S. M. Uosof, and S. N. Mohi, Iraqi J. Sci., 99 (2019).
19. N. Afsharimani, A. Durán, D. Galusek, and Y. Castro, Nanomaterials, **10**, 1050 (2020). DOI: https://doi.org/10.3390/nano10061050
20. Q. Kaddou and K. A. Al-Horani, Baghdad Sci. J. **2**, 533 (2021). DOI: https://doi.org/10.21123/bsj.2005.647
21. J. Abdi, M. Izadi, and M. Bozorg, Sci. Rep., **12**, 10660 (2022). DOI: https://doi.org/10.1038/s41598-022-14854-y
22. S. W. A. Aldeen, and N. M. Abbass, Chem. Methodol., **7**, 81 (2023). DOI: https://doi.org/10.22034/chemm.2023.357626.1598
23. R. Whba, M. S. Su'ait, F. Whba, and A. Ahmad, Journal of Power Scource, **606**, 234539 (2024). DOI: https://doi.org/10.1016/j.jpowsour.2024.234539
24. N. Liu, X. Zhang, E. He, W. Zhou, L. Yu, and X. Yan, Appl. Surf. Sci. **568**, 150937 (2021). DOI: https://doi.org/10.1016/j.apsusc.2021.150937.
25. Z. Momenzadeh, M. Ashjari, E. Nemati Lay, and M. Paki, Adv. Compos. Mater., **15** (2024). DOI: https://doi.org/10.1080/09243046.2024.2387413
26. D. Ahmed, and B.I. Al-Abdaly, Solid State Technology, **64**, 3945-3959 (2021).
27. A.A. Farag, Corrosion Reviews, **38**(1): 67 (2020). DOI: https://doi.org/10.1515/corrrev-2019-0011
28. N. Talavera, M. Navarro, A. Sifontes, Y.Díaz, H. Villalobos, G. Niño-Vega, and S.G. Pandalai, Recent research developments in materials science, **10**, 89 (2013).
29. Abdul-Zahra, M. A., & Abbass, N. M., Iraqi J. Sci., **65**, 623 (2024). DOI: https://doi.org/10.24996/ijs.2024.65.2.4.
30. Z. Z. Almarbd and N. M. Abbass, Chem. Methodol.,, **6**, 940 (2022). DOI: https://doi.org/10.22034/chemm.2022.359620.1603.
31. W. Hua, X. Xu, X. Zhang, H. Yan, and J. Zhang, J. Journal of Energy Storage, **56**, 105883 (2022). DOI: https://doi.org/10.1016/j.est.2022.105883

التخليق ومقاومة التآكل للمركبات النانوية القائمة على البولي أكريلونيتريل مع جزيئات النيكل وأكسيد الفاناديوم المستخرجة من المورينجا

ساره سعدي احمد[1] وندى مطير عباس[1]
[1]قسم الكيمياء، كليه العلوم، جامعه بغداد، بغداد، العراق

الخلاصة

يهدف هذا البحث إلى تحسين مقاومة التآكل للفولاذ الكربوني (السبائك 45) في المياه المالحة (3.5٪ NaClمن خلال تطبيق طلاء بوليمري نانوي. تم تصنيع المركب النانوي عن طريق دمج جسيمات نانوية من أكسيد النيكل (NiO) وأكسيد الفناديوم(V_2O_5)، والتي تم إنتاجها عبر طريقة تخليق خضراء باستخدام مستخلص المورينجا، في مصفوفة بولي أكريلونيتريل (PA) تم تقييم أداء الطلاء عبر نطاق من درجات الحرارة (293 كلفن، 303 كلفن، 313 كلفن، 323 كلفن)، حيث حقق فعالية تثبيط تصل إلى 89٪ عند 303 كلفن. تم توصيف المركبات النانوية المُصنعة باستخدام عدة تقنيات تحليلية، بما في ذلك المجهر الذري (AFM)، مطياف الأشعة تحت الحمراء بتحويل فورييه(FT-IR)، المجهر الإلكتروني النافذ(TEM)، حيود الأشعة السينية(XRD) ، التحليل الحراري الوزني(TGA)، والتحليل الحراري التفاضلي .(DSC) كشفت تحليلات AFM عن أحجام جزيئات تبلغ 44.5 نانومتر لأكسيد النيكل و 54.47 نانومتر لأكسيد الفناديوم، بينما أشارت صور TEM إلى مورفولوجيا كروية غير متجانسة. أكدت تحاليل FT-IR و XRDالدمج الناجح للجسيمات النانوية في مصفوفة البوليمر، وأظهرت تحليلات TGA/DSC الاستقرار الحراري للمركبات النانوية. تشير النتائج إلى أن هذه المركبات النانوية توفر إمكانية كبيرة كمثبطات فعالة للتآكل، مما يوفر حماية معززة للفولاذ الكربوني في البيئات المسببة للتآكل.

الكلمات المفتاحية: بولي أكريلونيتريل، مركب بوليمر، التخليق الأخضر،أكسيد النيكل النانوي، أكسيد الفناديوم الخماسي النانوي.